



Nanostructured niobium oxide synthetized by a new route using hydrothermal treatment: High efficiency in oxidation reactions

Nayara T. do Prado, Luiz C.A. Oliveira*

Departamento de Química, ICEX, Universidade Federal de Minas Gerais, Belo Horizonte, MG, CEP 31270-901, Brazil



ARTICLE INFO

Article history:

Received 13 September 2016

Received in revised form

13 December 2016

Accepted 28 December 2016

Available online 29 December 2016

Keywords:

Niobium oxide

Photocatalysis

Hydrothermal treatment

Oxidation

ABSTRACT

Nanostructured niobium oxides were synthesized by hydrothermal treatment using an amorphous Nb_2O_5 as precursor. The modification by hydrothermal treatment in the presence of oxalic acid or hydrogen peroxide resulted in versatile catalysts with many different properties verified by several characterization techniques. XRD analysis demonstrated the crystallinity increase. Significant morphological changes were observed by TEM, being possible to observe the presence of nanorods for the material treated with oxalic acid and nanospheres for the material treated in the presence of H_2O_2 . Modifications in the porous structure were also observed, as well as the increase in BET specific area. This significant difference compared to precursor resulted in catalysts with higher performance than Nb_2O_5 in decomposition of methylene blue dye (MB) by heterogeneous fenton-like reactions and photocatalysis under UV light irradiation.

© 2016 Elsevier B.V. All rights reserved.

1. Introduction

In the context of heterogeneous catalysis, it is observed that systems based on niobium have played an important catalytic role in several reactions, acting as active phase, dopant and also as support. Special features such as redox property, high acidity and strong metal-support interaction has enabled these systems to present high catalytic performance in several reaction types [1].

In view of this, several niobium oxide synthesis methodologies have been described in the literature. However, significant advancements have been made in tailoring niobium nanoparticles with controlled structures and morphologies due to the superior properties of nano-sized materials. The obtention of nano- Nb_2O_5 using the sol-gel method followed by calcination or precipitation method in aqueous ammonia is widely described in the literature. However, the hydrothermal method has been presented as a good strategy to obtain metal oxide nanocrystals using milder temperatures and reaction conditions [2–5].

Recently, several studies have reported that the use of coordinating small organic molecules, such as oxalic acid, have enabled better control of nucleation and morphology in the hydrothermal synthesis of nanomaterials based on TiO_2 and WO_3 aiming their application in photocatalysis [6,7]. This same structure-directing

agent was also employed in the hydrothermal synthesis of niobium oxide, allowing the obtention of nanocrystalline materials that showed a layered-type structure [8]. Moreover, there are several studies regarding the hydrothermal synthesis of Nb_2O_5 using alkaline solutions [9], but they mainly use niobic acid and niobium oxalate as the precursors.

In this work we report the synthesis of two catalysts obtained from the hydrothermal treatment, with oxalic acid or hydrogen peroxide, of a niobium oxide precursor in order to verify its influence on the morphology and porosity of the material. The advantage of using hydrogen peroxide lies in the fact that the only degradation products are water and oxygen. Therefore, it can be considered a clean synthesis method. Furthermore, hydrogen peroxide easily associates with transition metals such as Mo(VI), V(V), Nb(V) and W(VI), yielding metal-peroxo or metal-hydroperoxo species, which have received considerable attention due to their importance in a variety of industrial processes for showing the ability to release oxygen in active form [10]. Therefore, the proven catalytic properties of niobia and its availability justify the great interest in studying the behavior of this material in different processes.

The application of semiconductors in heterogeneous photocatalysis processes constitute an important research area. Currently, several studies have focused on developing new materials that are able to outperform TiO_2 , one of the most widely used nanostructured semiconductors.

* Corresponding author.

E-mail address: luioliveira@qui.ufmg.br (L.C.A. Oliveira).

Nb_2O_5 works under UV light irradiation as well as TiO_2 . Comparatively, TiO_2 is regarded as a benchmark photocatalyst and it shows several great advantages, like chemical stability, non-toxicity and commercial availability, which are also observed for niobium oxide. However, the literature describes the fact that the recombination rate of photo-generated hole-electron pairs on TiO_2 is very high, which greatly reduces the photocatalytic efficiency and limits the industrial application of TiO_2 [11].

Despite this, TiO_2 has the ability to form hydrocolloids with high stability in water, which favors the catalytic activity. On the other hand, such stability does not favor the separation of the photocatalyst from the water, making it difficult to recover and reuse, which is extremely important both from an environmental and economic point of view [12]. As Nb_2O_5 does not present this drawback, its use as photocatalyst can be a new alternative for the degradation of contaminants.

The work of Prado et al. can be mentioned as an example of the effective recyclability of niobium oxide. The authors reported better catalytic activity of Nb_2O_5 in relation to TiO_2 and ZnO in indigo carmine degradation after 10 reaction cycles, confirming the easy recovery and long-term stability of Nb_2O_5 in photocatalysis [12].

The existence of few studies concerning the use of Nb_2O_5 for photocatalytic applications makes its use of considerable interest for a better understanding of its mechanism of action and advantages over already established photocatalysts [13].

It is worth mentioning that photocatalysts have been shown high effectiveness in degrading harmful organic substances and, therefore they can be an interesting approach for the treatment of water and wastewater [14]. In view of the above, it was decided to evaluate the catalytic potential of the synthesized materials in the photodegradation of organic compounds using methylene blue as a model molecule.

Other methods of chemical decomposition of organic contaminants are the Fenton-like systems, in which hydroxyl radicals can be generated by direct interaction of metal-hydroxyl species with H_2O_2 [15]. Despite the hydroxyl radicals belonging to the most reactive chemical species, metal peroxy and metal oxo-species also have been shown to be active intermediates in the oxidation of organic compounds [16]. Thus, the catalysts synthesized here were also assessed in Fenton-like systems since the possible generation of peroxy groups, after the hydrothermal treatment with H_2O_2 , can confer good catalytic performance in the reaction mentioned type. In this way, the reactional systems reported here demonstrate the great potential and versatility possessed by niobium-based systems. However, their preparation, in the nanostructured form with high surface area, still represents a big challenge, evidencing the need for further studies in this area.

2. Experimental

2.1. Synthesis of the catalysts

Nb_2O_5 nanoparticles with different morphologies were synthesized by the hydrothermal method using a BERGHOF® BR-100 stainless steel autoclave containing a Teflon cup and magnetic stirrer set at 300 rpm. 1 g of Nb_2O_5 (supplied by CBMM) was dispersed in 40 mL of oxalic acid solution (OX) (0.2 mol L^{-1}) or 40 mL of distilled water and a subsequent addition of hydrogen peroxide (HP) (Synth, 50% v/v) in a 10:1 H_2O_2 :Nb molar ratio. The suspension was placed in hydrothermal cell and the temperature adjusted to 220 °C for the treatment with OX or 150 °C for the treatment with HP under autogenous pressure in both cases. The times of the hydrothermal synthesis were 4 h for the OX treatment and 12 h for the treatment with HP, the materials identified as Nb_2O_5 -OX, and Nb_2O_5 -HP, respectively. These treatment times were chosen

based on previous studies of our research group [17]. The solids obtained as final products were washed with distilled water until pH = 7, centrifuged and dried at 70 °C for 12 h.

2.2. Catalytic reactions

The photocatalytic activity of the synthesized materials was evaluated by the degradation of methylene blue dye (MB) under UV light irradiation. For this purpose, 10 mg of the catalyst was added to 10 mL of a MB aqueous solution (20 mg L^{-1}). Before irradiation, the photocatalyst was dispersed by magnetic stirring in absence of light for 60 min to achieve adsorption–desorption equilibrium between the photocatalyst and MB. Thereafter, the suspension was irradiated with UV light. The times of 30, 60, 120, 180, 240 and 300 min were evaluated. After centrifugation to separate the photocatalyst particles, the supernatants were analyzed at 664 nm using a UV-2600 Shimadzu spectrophotometer.

In Fenton-like systems, the oxidation of the methylene blue dye (50 mg L^{-1}) was carried out in the presence of 0.1 mL of H_2O_2 (Synth, 50% v/v), with a total volume of 10 mL and 10 mg of the catalyst during 5, 10, 30, 45, 60 and 120 min. As in the photocatalytic tests, the conversions were monitored by UV–vis measurements at 664 nm.

Total organic carbon content (TOC) was performed with a Shimadzu TOC-V_{CPH}, in order to evaluate the mineralization of the MB.

2.3. Characterization of the materials

UV–vis spectroscopy with diffuse reflectance geometry was performed with a UV-2600 Shimadzu from 200 to 800 nm. BaSO_4 powder was used as a reference (100% transmission), and the Kubelka–Munk equation was employed to manipulate the data.

X-ray diffraction data (XRD) was collected using a scan rate of 1° min^{-1} on a Shimadzu equipment, model XRD-7000 X-ray diffractometer, equipped with copper tube, 30 mA current and 30 kV voltage.

Transmission electron microscopy of the samples was carried out using Tecnai G2-20-SuperTwin FEI-200 kV at the Microscopy Center – UFMG.

The specific surface areas of the catalysts were calculated through the BET method in a low relative pressure region using the technique of adsorption/desorption of nitrogen at 77 K in a Quantachrome Autosorb iQ₂ equipment. The pore size distribution was calculated from the isotherm using the BJH model and the NLDFT method.

The acidity properties of the catalysts were characterized by the Temperature Programmed Desorption method (TPD) using NH_3 as probe molecule. A Quantachrome ChemBET-3000 equipment, containing TCD detector using a current of 150 mA and an attenuation of 32, was used. Approximately 0.2 g of catalyst was treated at 100 °C for 60 min in a continuous helium flow (80 mL min^{-1}) and NH_3 adsorption was then conducted at 50 °C. The TPD- NH_3 profiles were obtained at a heating rate of $10^\circ \text{ C min}^{-1}$.

The identification of acid sites of the samples was performed by adsorption of pyridine followed by infrared spectroscopy. Approximately 10 mg of sample was treated at 100 °C for 2 h under $\text{N}_2(\text{g})$ flow (80 – 100 mL min^{-1}). Then the pyridine adsorption was carried out at a temperature of 55 °C for 1 h. Subsequently, the physisorbed pyridine was removed by heating the catalysts at 100 °C for 1 h. The samples were prepared as KBr pellets and analyzed by infrared spectroscopy in the 1800 – 1400 cm^{-1} region with resolution of 4 cm^{-1} and 16 scans.

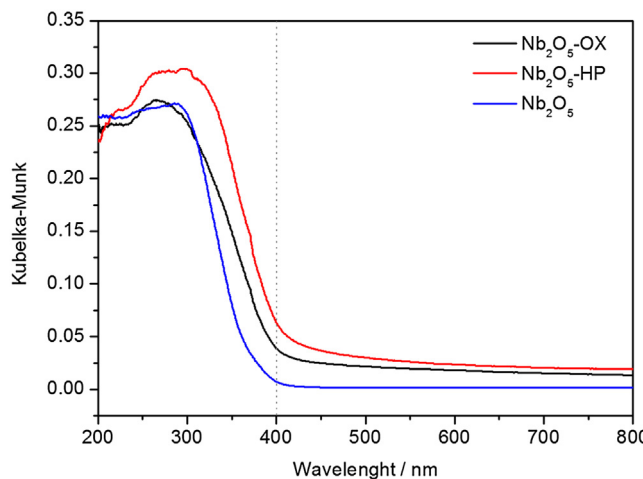


Fig. 1. UV-vis diffuse reflectance spectra of samples raw Nb_2O_5 , Nb_2O_5 -OX and Nb_2O_5 -HP.

3. Results and discussion

3.1. Characterization of the catalysts

UV-vis diffuse reflectance measurement was used to investigate the electronic structure of the catalysts raw Nb_2O_5 , Nb_2O_5 -OX and Nb_2O_5 -HP, which is of significant importance to the photocatalysis. Diffuse reflectance UV-vis spectra of the catalysts (Fig. 1) demonstrate that materials absorb in the ultraviolet region. It was also observed that the hydrothermal treatment afforded a significant increase in absorbance related to the Nb_2O_5 -HP material as compared to the precursor Nb_2O_5 . This increase in the intensity of the absorption line, especially in the range of 300–400 nm, is assigned to electron transfer from O_2^- to Nb and indicates the interactions of niobium with hydrogen peroxide [18], demonstrating that the treatment was able to produce the peroxy groups, as proposed in our previously work [17].

The band gap energies for the materials were calculated using the equation considering the indirect transition to the semiconductor ($n=4$): $\alpha h\nu = A(h\nu - E_g)^{n/2}$. In this equation, α , $h\nu$, A , E_g and n are the absorption coefficient, Planck's constant, light frequency, proportionality constant, band gap energy and the transition order in a semiconductor, respectively. The estimated band gaps of Nb_2O_5 , Nb_2O_5 -OX and Nb_2O_5 -HP are 3.6 eV, 3.3 eV and 3.2 eV, respectively. As can be seen, the hydrothermal treatment also provided change in the electronic structure of the materials, making their band gap values smaller than that of its precursor.

The X-ray diffraction patterns of the catalysts synthesized under hydrothermal conditions reveal a short-range order and a significant increase in the crystallinity when compared to the precursor Nb_2O_5 (Fig. 2). Such behavior is usually attributed to the rearrangement of the niobium polyhedral units caused by the occurrence of dissolution and recrystallization during the hydrothermal synthesis process [8]. The phases were identified using the Powder Diffraction File (PDF) database (JCPDS, International Centre for Diffraction Data).

The reflections only showed the Nb_2O_5 phase. Furthermore, using the Scherrer equation there are crystallite sizes of approximately 12 nm for the starting Nb_2O_5 , 11 and 14 nm for the materials treated hydrothermally, i.e., Nb_2O_5 -HP and Nb_2O_5 -OX, respectively. The small crystallite size shows that these materials can be active as catalysts, even after the hydrothermal treatment there was no significant increase in the size of materials.

The morphology of the catalysts was evaluated by transmission electron microscopy (TEM) (Fig. 3). The images show that the use of

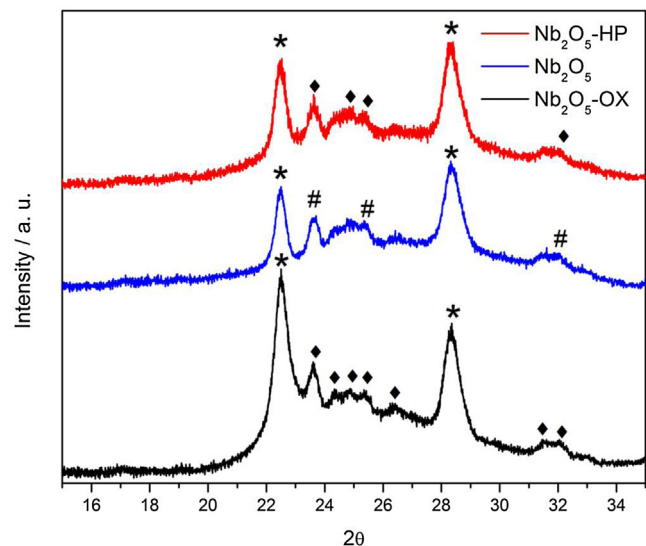


Fig. 2. X-ray Diffraction of the catalysts (* = Nb_2O_5 (JCPDS-ICDD file 27-1312); ♦ = Nb_2O_5 (JCPDS-ICDD file 30-872); # = Nb_2O_5 (JCPDS-ICDD file 19-862)).

structure-directing agents, in combination with the hydrothermal treatment, allowed the production of materials containing different morphologies and crystalline regions, supporting the data obtained by X-ray diffraction.

The presence of nanorods was verified for the Nb_2O_5 -OX material. Image J software was used for processing the images. The particle size distribution showed an average diameter of 6 nm (Fig. 3). Measurements of interplanar spacing were also performed and the value of 0.376 nm for Nb_2O_5 -OX correlates with the third largest reflection observed in the XRD diffractogram, centered at 23.6°, being identified according to the JCPDS-ICDD file 30-872.

According to the literature [6], the use of oxalic acid prevents the formation of skewed chains due to their chelation to metal polyhedral through oxygen atoms. This allows the careful control of recrystallization processes to template the nanorod growth. A similar morphology has been described for tungsten and titanium oxides also synthesized under hydrothermal conditions in the presence of oxalic acid [19,20]. This particular morphology can significantly contribute to catalysis, since the formation of interparticle pores occurs, facilitating the diffusion of molecules. Moreover, this type of morphology favors the appearance of defects on the edges, which can also be a factor in favor of catalytic reactions.

On the other hand, spherical nanoparticle agglomerates were produced in the Nb_2O_5 -HP material. This feature made it difficult to measure the average particle size, and therefore, only the interplanar spacing data are presented here. It should be noted that the values of 0.395 nm and 0.316 nm correlate to the two most intense reflections observed in the XRD diffractogram, centered at 22.48° and 28.21°, respectively. These reflections correspond to the (0 4 0) and (0 5 0) planes of the monoclinic system of Nb_2O_5 , respectively, according to the JCPDS-ICDD file 27-1312.

The use of H_2O_2 is advantageous because it does not generate toxic by-products or contaminants that could interfere in the catalytic tests.

Fig. 4 shows the N_2 adsorption/desorption isotherms of the samples, as well the pore size distribution profile obtained by the Barrett-Joyner-Halenda method (BJH). According to the original IUPAC classification [21], isotherms are similar in behavior to Type IV. The assigned classification indicates multilayer adsorption of mesoporous solids. Nb_2O_5 -OX and Nb_2O_5 -HP show distinct textural properties compared to raw Nb_2O_5 . The hydrothermal

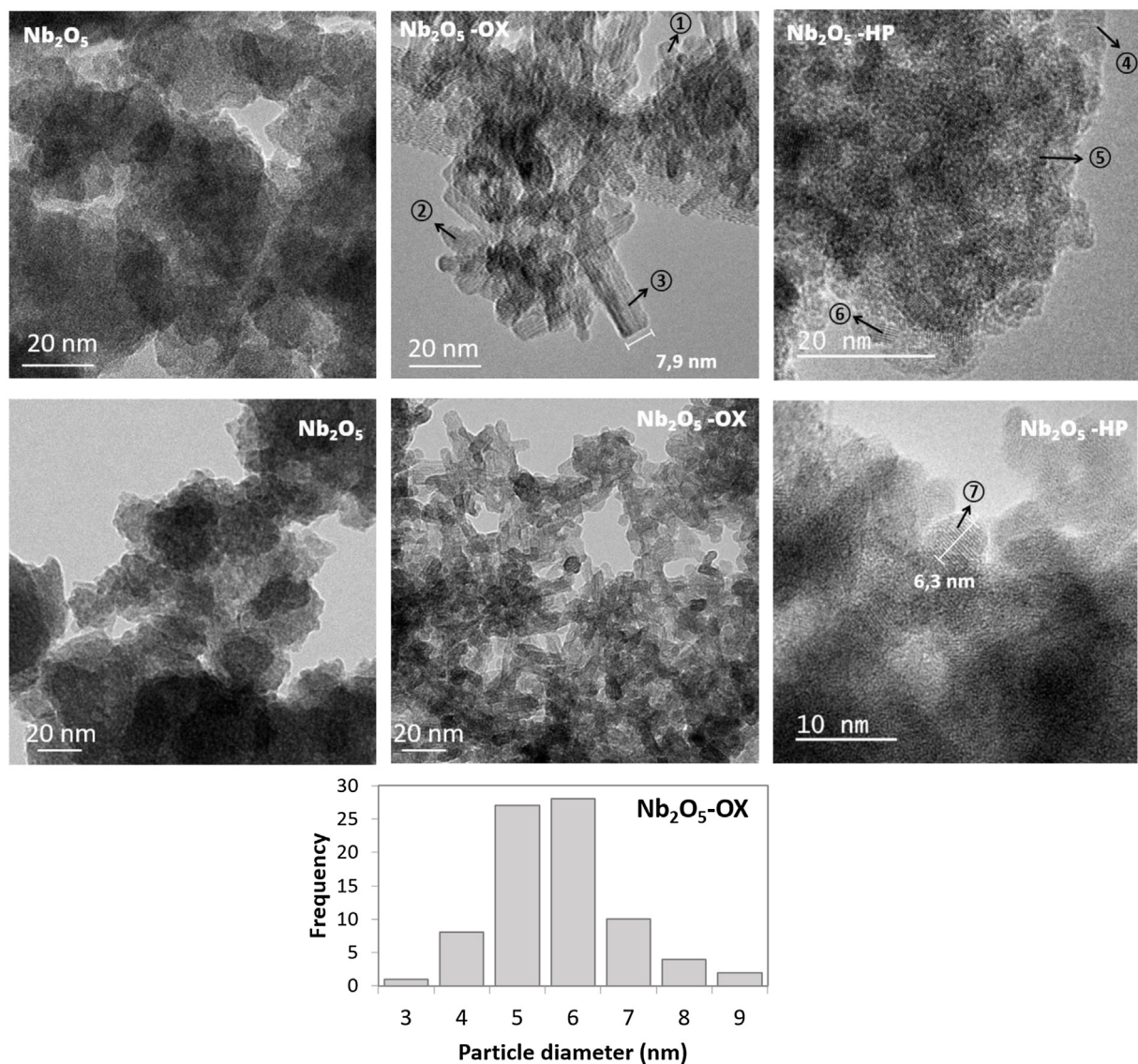


Fig. 3. Transmission electron microscopy images for the catalysts Nb₂O₅, Nb₂O₅-OX and Nb₂O₅-HP and particle size distribution histogram of the Nb₂O₅-OX sample. Values of interplanar spacing: (1)=0.425 nm; (2)=0.376 nm; (3)=0.428 nm; (4)=0.316 nm; (5)=0.311 nm; (6)=0.395 nm; (7)=0.311 nm.

treatment resulted in materials with larger pore diameters and higher BET specific area.

The isotherm related to the Nb₂O₅-OX catalyst exhibited a hysteresis that resembles the H3 model proposed by IUPAC, which is caused by the existence of non-rigid aggregates of plate-like particles, which originate pores in wedge shapes, cones or parallel plates. This result is related to the one obtained through TEM, whose material presented particles in the form of nanorods/parallelepipeds [22]. It is observed, therefore, that the chosen directing agents decisively influence the textural properties.

Despite BJH method being the standard procedure for calculating the pore size distribution in mesoporous materials, several publications have reported that BJH may underestimate or overestimate the pore size in the range of nanopores [23,24].

Its lower accuracy stems from the fact that thermodynamics based methods like BJH fail to account for molecular size effects that become important for small pores [24].

Due to the different adsorption mechanisms involved and the wide range of pore sizes that porous materials may present, new methods continue to be developed to provide greater accuracy in

pore size distribution (PSD). In this sense, the NLDFT (Non-Local Density Functional Theory) method was used to determine the pore size distribution of the catalysts reported in this study. NLDFT takes into consideration gas-surface interactions on atomistic level of detail and has been developed to evaluate the pore size distribution of microporous and mesoporous materials [25].

In this work, the ASiQwin software, v.3.0 (Quantachrome Instruments) was applied in order to obtain the PSD by NLDFT method. The kernel selected was that referring to N₂ at 77 K on silica, using the adsorption branch.

As can be observed in Fig. 4, there are significant differences in the pore size distribution curves assessed by the NLDFT and BJH methods. The maximum points of the curves are slightly different, with larger values of pore size being obtained by the NLDFT method. In addition, the results reinforce the mesoporous characteristics of the materials, as previously reported, since the NLDFT method did not indicate the presence of micropores.

Pyridine adsorption, followed by infrared spectroscopy, was used for identification of acid sites in the samples. This feature was evaluated since some studies have reported the possibility of immobilizing the dye species by acid sites [13].

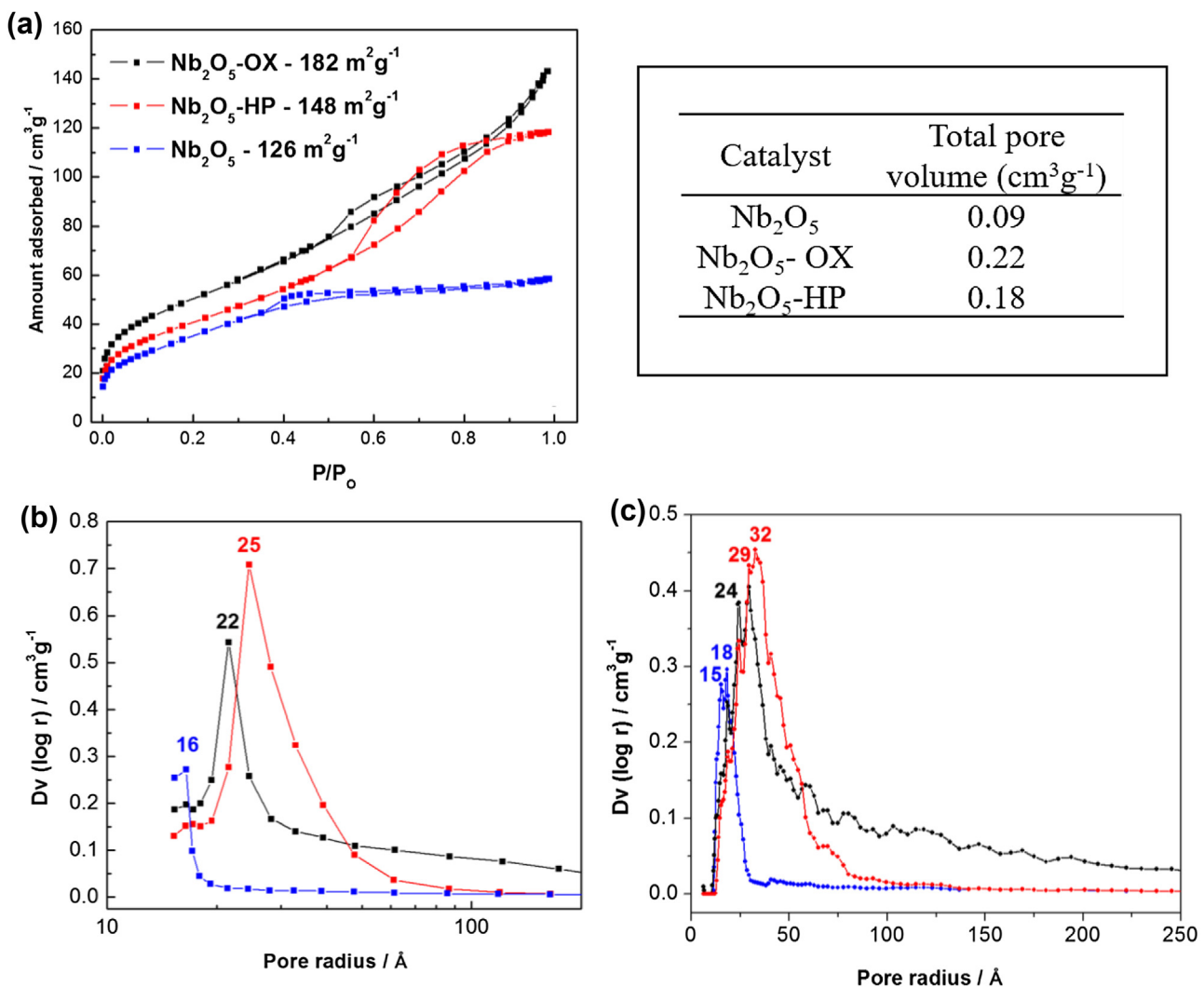


Fig. 4. (a) N₂ adsorption/desorption isotherms, total pore volume of catalysts and the respective pore size distribution by (b) BJH and (c) NLDFT.

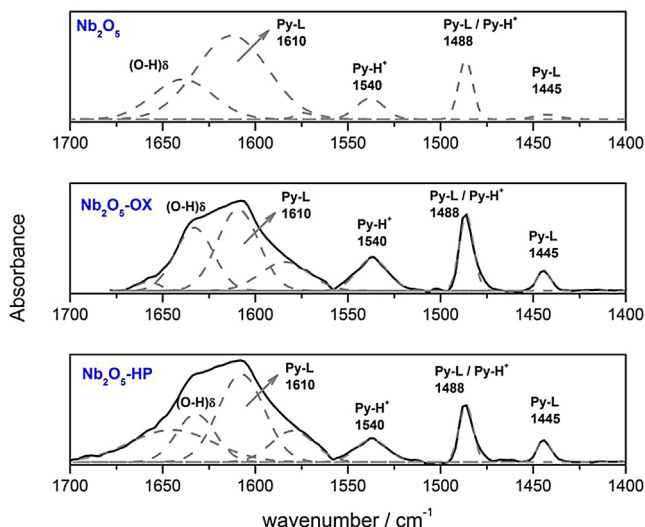


Fig. 5. Infrared spectra obtained after pyridine adsorption in catalysts.

The spectra presented in Fig. 5 show, in particular, four quite peculiar bands. The first at 1540 cm⁻¹ is assigned to the vibrational mode of the pyridinium ion (Py-H⁺, Bronsted sites). The bands at

Table 1

Areas of the bands corresponding to the vibrations of coordinated pyridine (1445 cm⁻¹) and protonated pyridine (1540 cm⁻¹) and the number of total acid sites (TPD-NH₃).

Catalyst	Area (a.u.) Py-L (1445 cm ⁻¹)	Area (a.u.) Py-H ⁺ (1540 cm ⁻¹)	Number of acid sites (μ mol g ⁻¹) ^a
Nb ₂ O ₅	0.301	1.464	18
Nb ₂ O ₅ -OX	0.685	2.502	58
Nb ₂ O ₅ -HP	0.755	1.799	49

^a Number of acid sites determined by TPD-NH₃ from the standard beta zeolite with a specified number of sites of 472 μ mol g⁻¹ [27].

1445 cm⁻¹ and 1610 cm⁻¹ correspond to the vibrational mode of pyridine coordinated to Lewis acid sites (Py-L). Finally, the band at 1488 cm⁻¹ corresponds to vibrational modes of both the protonated and coordinated pyridine [26].

The highest band area values at 1445 cm⁻¹ and 1540 cm⁻¹ (usually used in the quantification of acid sites) for the catalysts Nb₂O₅-OX and Nb₂O₅-HP (Table 1) shows that there was an increase in acidity after the hydrothermal treatment, which is a result coincident with the NH₃-TPD data presented in Table 1.

The significant value for the BET area of niobium compounds reported herein, as well as the mesoporous character displayed by the catalysts, are very desirable properties for good performance in catalytic reactions. Larger pore size could facilitate the diffusion

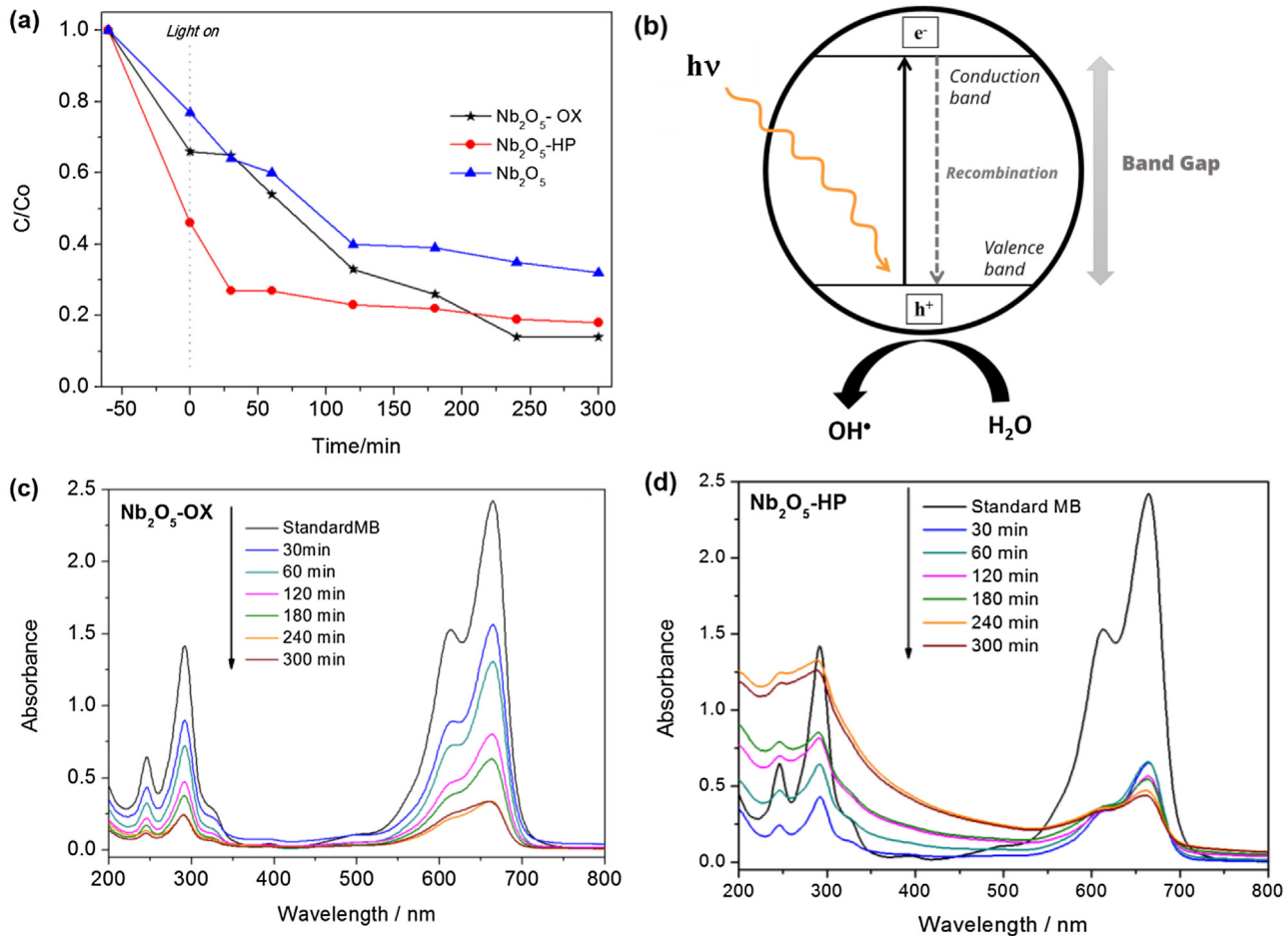


Fig. 6. (a) Photodegradation of methylene blue, in an aqueous solution, by Nb_2O_5 , Nb_2O_5 -OX and Nb_2O_5 -HP as a function of exposure time to UV irradiation. (b) Schematic representation of electron-hole pair. (c) UV/Vis absorption curves of methylene blue versus UV irradiation time with Nb_2O_5 -OX, and (d) Nb_2O_5 -HP.

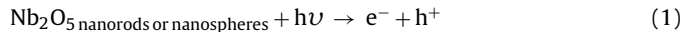
of methylene blue molecules and higher surface areas could offer more active sites for adsorption, resulting in more efficient photocatalytic reaction. The differences in the pore size distribution profile can be assigned to the different morphologies induced by the particle growth process during the hydrothermal synthesis, as observed by TEM analyses.

3.2. Photocatalysis and Fenton-like reactions: oxidative properties of the catalysts

The versatility of the materials can be probed according to: (i) their capacity of activated H_2O_2 to generate $\bullet\text{OH}$ radical or formation of surface peroxy groups, which are strongly oxidizing species. Both can act as strongly oxidizing species [28–30]; (ii) their activity to produce $\bullet\text{OH}$ radical by photocatalytic process under UV light, since the materials have semiconductor properties. It was decided to evaluate the activity of materials based on Nb_2O_5 in decomposition of methylene blue dye (MB) in aqueous solution, which is a molecule intensely used as a model in various studies [31]. For this purpose, the heterogeneous Fenton-like and photocatalysis were carried out because they are two of the most studied technologies used for the removal of contaminants.

Band gap values shown previously are related to the results obtained by the photocatalytic tests. As seen in Fig. 6(a), the removal of methylene blue by photocatalysis using UV light irradiation reached 86, 82 and 68% in the presence of Nb_2O_5 -OX, Nb_2O_5 -HP and Nb_2O_5 , respectively, after 5 h. This result was also associated

with an increase of the hydrothermal Nb_2O_5 exposed surface area available per molecule of MB. Nb_2O_5 nanorods or nanospheres synthetized in this work present a broad absorption band between 200 and 350 nm. In this sense, when hydrothermal catalysts were irradiated with UV light with energy higher than the band gap, electrons (e^-) were photo-induced to conduction, generating holes (h^+) in the valence bands. The holes can be trapped to produce the hydroxyl radical species (Fig. 6(b)). In addition, intrinsic defects in the crystal structure were created in the semiconductor since they are favoured by the synthesis of the nanoparticles under the hydrothermal condition. They can act as intermediate energy states for the electrons, inhibiting or delaying the rapid carrier recombination processes, thus improving the separation of electron-hole pairs (Eqs. (1)–(4)) [31].



Although UV-vis spectroscopy does not provide any information about MB degradation reaction intermediates, it enables the observation of the structural transformation of MB during the reaction. As presented in Fig. 6(c) and (d), the band in the visible region observed at 664 nm is correlated with the chromophore groups of the dye. Therefore, a decrease in its intensity reflects the discolouration of the solution and consequently the concentration of MB in solu-

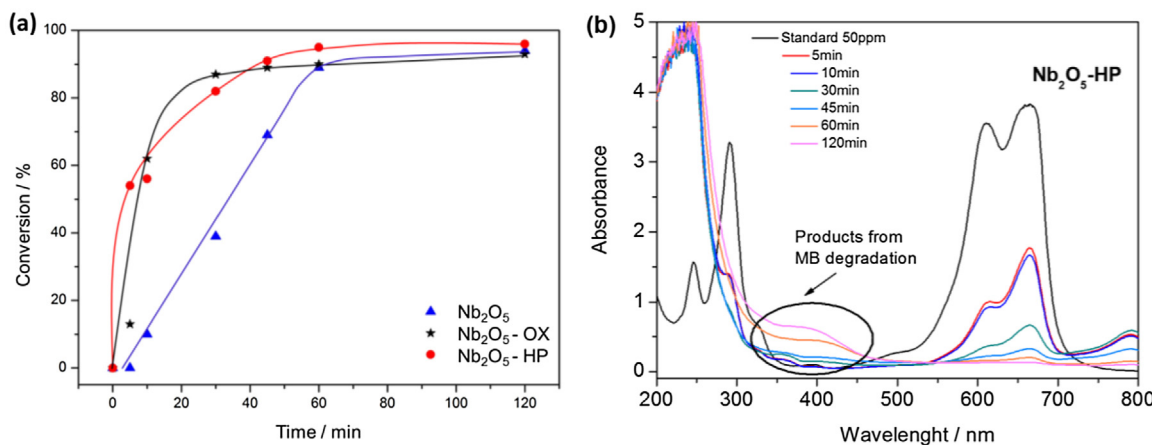


Fig. 7. (a) Degradation kinetics of methylene blue (50 mg L^{-1}) by Nb_2O_5 , $\text{Nb}_2\text{O}_5\text{-OX}$ and $\text{Nb}_2\text{O}_5\text{-HP}$ in the presence of H_2O_2 and (b) the respective UV-vis spectra for Fenton-like reactions using $\text{Nb}_2\text{O}_5\text{-HP}$.

tion. Moreover, the bands in the ultraviolet region are assigned to benzene-like structures, so that the decrease of absorbance of these bands, as the reaction proceeds, indicate that benzene and naphthalene rings were degraded to other compounds and eventually CO_2 and water.

Moreover, the degree of adsorption on the materials was assessed in the absence of a light source. Hydrothermal catalysts exhibited a stronger affinity for the dye molecules than the precursor. This behavior can be related to the acid groups of the materials $\text{Nb}_2\text{O}_5\text{-OX}$ and $\text{Nb}_2\text{O}_5\text{-HP}$, previously discussed. As related in the literature, the dye species are immobilized by the solid acid sites. The nucleophilic moieties of methylene blue, such as lone pair electrons in nitrogen and sulfur may adsorb on the Lewis acidic Nb^{5+} sites before irradiation. Thereby, the photoinduced electrons and holes on the surface can attack the molecules [13].

A comparison of the MB conversion versus time for the catalysts Nb_2O_5 , $\text{Nb}_2\text{O}_5\text{-OX}$ and $\text{Nb}_2\text{O}_5\text{-HP}$ in the presence of H_2O_2 (in absence of light) is shown in Fig. 7(a). These results demonstrate the remarkable efficient Fenton-like degradation toward MB presented by hydrothermal catalysts.

As can be seen in the temporal evolution of UV-vis spectra for $\text{Nb}_2\text{O}_5\text{-HP}$ (Fig. 7(b)), the band at 664 nm (corresponding to monomer absorption) is practically extinguished after 120 min. The intense absorption at about 400 nm, can be related to the new compounds generated from MB oxidation. This results indicates that the MB molecule can form fragments after reactions with the $\cdot\text{OH}$ radicals produced by the Fenton-like process and/or by oxidation by peroxy groups on the surface. The Eqs. (5) and (6) illustrates the reactions mentioned above.

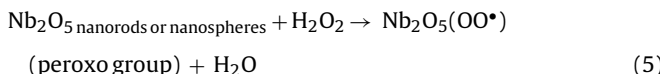


Fig. 7(a) also shows that when considering the same time period (30 min), the hydrothermally synthesized materials allowed to obtain almost double the conversion that was obtained using the precursor Nb_2O_5 .

As presented previously, the disappearance of the MB was monitored by UV-vis spectroscopy. Although the discoloration of the solution and, consequently, the decrease in concentration of MB in solution were observed, measurements of total organic car-

bon (TOC) were also carried out to determine the carbon content present in the solution after the catalytic process.

This is an important data since colorless organic subproducts can be formed during the reaction in addition to the products of complete degradation of MB (like gaseous CO_2). TOC measurements were made for the reactions carried out with the $\text{Nb}_2\text{O}_5\text{-OX}$ catalyst at the highest reaction times (120 min for Fenton and 300 min for photocatalysis).

Results demonstrate that the photocatalysis promoted a higher mineralization of methylene blue (approximately 83%) in relation to the Fenton process (72% of mineralization).

It is interesting to comment that the TOC removal results presented above were better than those reported by some authors [32,33], attesting that the materials described in this study are good catalysts in the oxidation of an important organic pollutant such as methylene blue.

4. Conclusions

Nb_2O_5 nanostructures have been successfully prepared by hydrothermal treatment using different structure-directing agents (oxalic acid and hydrogen peroxide). The characterization of these new materials showed that they exhibited differentiated properties compared to its precursor Nb_2O_5 . The nanostructured niobium oxide presented morphologies in the form of rods or spheres, as well as higher crystallinity, lower band gap values and the modification of porous properties with increase in BET area.

In the catalytic context, Nb_2O_5 nanostructures synthesized were found to be effective catalysts for Fenton-like reactions and active photocatalysts under UV light irradiation in degradation of methylene blue dye. The best result for Fenton-like reactions indicated the removal of 80% of MB in just 30 min using the $\text{Nb}_2\text{O}_5\text{-HP}$ catalyst and a 50 ppm dye concentration. The photocatalysis tests using UV light irradiation provided the removal of up to 86% of MB after 5 h using the $\text{Nb}_2\text{O}_5\text{-OX}$ catalyst.

As such, the results described herein demonstrate that the synthesis method employed provides an easy route for synthesizing low cost and stable nanocatalysts based on niobium oxide.

Acknowledgements

The authors gratefully acknowledge Capes, CNPq e FAPEMIG for financial support, as well as the Microscopy Center-UFMG and CBMM.

References

- [1] M. Ziolek, *Catal. Today* 78 (2003) 47–64.
- [2] Y. Zhou, Z. Qiu, M. Lü, A. Zhang, Q. Ma, *Mater. Res. Bull.* 43 (2008) 1363–1368.
- [3] R. Brayner, F. Bozon-Verduraz, *Phys. Chem. Chem. Phys.* 5 (2003) 1457–1466.
- [4] M. Ristić, S. Popović, S. Musić, *Mater. Lett.* 58 (2004) 2658–2663.
- [5] E.R. Camargo, M.G. Dancini, *J. Mater. Res.* 29 (2013) 131–138.
- [6] Q.D. Truong, T.H. Le, J.-Y. Liu, C.-C. Chung, Y.-C. Ling, *Appl. Catal. A: Gen.* 437–438 (2012) 28–35.
- [7] L. Li, J. Zhao, Y. Wang, Y. Li, D. Ma, Y. Zhao, S. Hou, X. Hao, *J. Solid State Chem.* 184 (2011) 1661–1665.
- [8] T. Murayama, J. Chen, J. Hirata, K. Matsumoto, W. Ueda, *Catal. Sci. Technol.* 4 (2014) 4250–4257.
- [9] H. Zhu, Z. Zheng, X. Gao, Y. Huang, Z. Yan, J. Zou, H. Yin, Q. Zou, S.H. Kable, J. Zhao, Y. Xi, W.N. Martens, R.L. Frost, *J. Am. Chem. Soc.* 128 (2006) 2373–2384.
- [10] D. Bayot, M. Devillers, *Coord. Chem. Rev.* 250 (2006) 2610–2626.
- [11] J. Yan, G. Wu, N. Guan, L. Li, *Appl. Catal. B: Environ.* 152–153 (2014) 280–288.
- [12] A.G.S. Prado, L.B. Bolzon, C.P. Pedroso, A.O. Moura, L.L. Costa, *Appl. Catal. B: Environ.* 82 (2008) 219–224.
- [13] Y. Zhao, C. Eley, J. Hu, J.S. Foord, L. Ye, H. He, S.C.E. Tsang, *Angew. Commun.* 51 (2012) 3846–3849.
- [14] S. Ahmed, M.G. Rasul, W.N. Martens, R. Brown, M.A. Hashib, *Water Air Soil Pollut.* 215 (2011) 3–29.
- [15] E. Jorda, A. Tuel, R. Teissier, J. Kervennal, *J. Catal.* 107 (1998) 93–107.
- [16] M. Ziolek, *Catal. Today* 90 (2004) 145–150.
- [17] N.T. Prado, T.E. Souza, A.R.T. Machado, P.P. Souza, R.S. Monteiro, L.C.A. Oliveira, *J. Mol. Catal. A: Chem.* 422 (2016) 23–34.
- [18] M. Ziolek, I. Sobczak, P. Decyk, L. Wolski, *Catal. Commun.* 37 (2013) 85–91.
- [19] V.B. Patil, P.V. Adhyapak, S.S. Suryavanshi, I.S. Mulla, *J. Alloys Compd.* 590 (2014) 283–288.
- [20] M. Wang, Q. Zeng, B. Zhao, C. Chen, G. Liu, D. He, *Catal. Commun.* 48 (2014) 60–64.
- [21] F. Rouquerol, J. Rouquerol, K.S.W. Sing, P. Llewellyn, G. Maurin, *Adsorption by Powders and Porous Solids. Principles, Methodology and Applications*, second ed., Elsevier, 2014.
- [22] M. Kruk, M. Jaroniec, *Chem. Mater.* 13 (2001) 3169–3183.
- [23] P.I. Ravikovich, G.L. Haller, A.V. Neimark, *Adv. Colloid Interface Sci.* 76–77 (1998) 203–226.
- [24] S. Lowell, J.E. Shields, M.A. Thomas, M. Thommes, *Characterization of Porous Solids and Powders: Surface Area, Pore Size and Density*, Kluwer Academic Publishers, 2004.
- [25] A.L. Kolesnikov, H. Uhlig, J. Möllmer, J. Adolpfs, Y.A. Budkov, N. Georgi, D. Enke, R. Gläser, *Microporous Mesoporous Mater.* 240 (2017) 169–177.
- [26] I.A.L. Bassan, D.R. Nascimento, R.A.S. San Gil, M.I.P. Da Silva, C.R. Moreira, W.A. Gonzalez, A.C. Faro Jr., T. Onfroy, E.R. Lachter, *Fuel Process. Technol.* 106 (2013) 619–624.
- [27] S.R. Amador, *Estudio del sistema Pt/zeolita+alúmina en las reacciones de reformación de gasolinas*, Universidad Autónoma Metropolitana, 2000.
- [28] F.G.E. Nogueira, J.H. Lopes, A.C. Silva, M. Gonçalves, A.S. Anastácio, K. Sapag, L.C.A. Oliveira, *Appl. Clay Sci.* 43 (2009) 190–195.
- [29] W. Ferraz, L.C.A. Oliveira, *Catal. Commun.* 8 (2007) 131–134.
- [30] J.V. Coelho, M.S. Guedes, R.G. Prado, J. Tronto, J.D. Ardisson, M.C. Pereira, L.C.A. Oliveira, *Appl. Catal. B: Environ.* 144 (2014) 792–799.
- [31] A.A.P. Mansur, H.S. Mansur, F.P. Ramanery, L.C. Oliveira, P.P. Souza, *Appl. Catal. B: Environ.* 158–159 (2014) 269–279.
- [32] A. Sandoval, C. Hernández-ventura, T.E. Klimova, *Fuel* (2016) (in press).
- [33] Y. Yang, L. Xu, H. Wang, W. Wang, L. Zhang, *Mater. Des.* 108 (2016) 632–639.